Vertical Flight Society

2020 – 2021 Design-Build-Vertical Flight Competition

Final Technical Report

March 29th, 2021

Executive Summary

Buckeye Vertical, a student organization at The Ohio State University, was founded to give students the opportunity to explore Advanced Air Mobility (AAM) and Unmanned Aircraft Systems (UAS). One of Buckeye Vertical's main goals is to give students the opportunity to explore and understand this field of study through professional development opportunities and project-based competitions that will support and create a platform of academic enrichment and excellence. AAM is a rapidly growing field and Buckeye Vertical strives to spread awareness and engage the student and Columbus community in a variety of ways regarding vertical flight technology.

The purpose of participation is to build an electric vertical take-off and landing (eVTOL) aircraft and understand its application in the field of Aerospace while developing a report to document the technical intricacies, engineering design challenges, and decisions approached throughout the project. Major design drivers were first mapped out based on the scoring of the competition and established parameters that would guide major decisions. The team designed an aircraft to maximize competition scoring. Goals were set for parameters affecting scoring such as the aircraft's cruising speed, hover time, and weight. The team was able to begin making predictions for the performance and calculations to set design requirements such as minimum thrust, wing performance, and required power draw. Various UAS configurations were considered, and the team narrowed the selection to three final configuration concepts. The three configurations were a quadcopter, hexacopter, and fixed wing tilt rotor design. The team chose to design and build a fixed wing tilt rotor after comparing the design requirements of each configuration with the performance challenges using a house of quality table.

After conducting research on the tilt rotor UAS configuration, conceptual calculations determined the design requirements governing the aircraft's design. By analyzing the force balance on a body, predictions were made for the required rotor thrust and/or wing lift in each of the flight modes of the tilt rotor quadcopter. These modes are takeoff, transition, horizontal flight, and landing. The team utilized the engineering and design process to finalize a design for the aircraft. First, the aircraft design requirements were consolidated during the modeling phase in SolidWorks. The concept of structural integrity vs. weight was emphasized during the design process to correctly select the best materials for the aircraft. Key sub-assemblies including the wing, motor booms, and fuselage were designed separately and later combined into a complete aircraft design. The team developed innovative solutions for the tilt rotor mechanism and wing design for the aircraft after multiple iterations of the design process to allow for maximum efficiency during flight. Aerodynamic analysis conducted with XFLR5 software aided in designing a wing that met the required performance parameters in horizontal flight.

A structural analysis for the aircraft design was also performed to ensure the booms could withstand the aircraft's weight, thrust, and max G-Forces involved during flight. Bolted-joint analysis calculations were also performed to make sure proper size bolts and brackets were used to assemble the aircraft's frames. The reasoning behind the decision to use GR-10/FR4 instead of carbon fiber for the main fuselage frame was also explained by comparing the cost savings and small material specification discrepancies between the two. An analysis of the 3-D printed blocks supporting the booms were also performed to assess the maximum forces the aircraft could withstand before tearout would occur.

The team developed a final parts list to complete the assembly of the aircraft. These parts were selected based on their ability to meet or exceed performance requirements set by the design calculations. This included a comparison and analysis of materials used. During assembly, the team utilized various fabrication techniques including CNC machining and 3-D printing to customize certain parts for the assembly. Finally, the team was able to prepare for final assembly by checking for needed assembly materials and looking for potential integration issues and resolving them before they could stall work on the aircraft. Assembly took place in a lab over several build days, as well as some take-home assembly work. The sub-teams worked together and separately depending on what needed to be accomplished at a particular time in the build process.

Calculations were made to predict mission performance with the selected aircraft performance. These calculations will be used to compare the ideal performance to the actual performance found during flight testing. Sub-system tests, such as avionics power/operation tests and software simulations, were another method of getting ahead of potential issues as early as possible. The team aimed to quickly be able to test the aircraft capabilities during a strict flight-testing agenda. This testing allows for collection of qualitative and quantitative data to reveal issues with the current aircraft that may need fixed and to guide discussion and provide data for future eVTOL iterations.

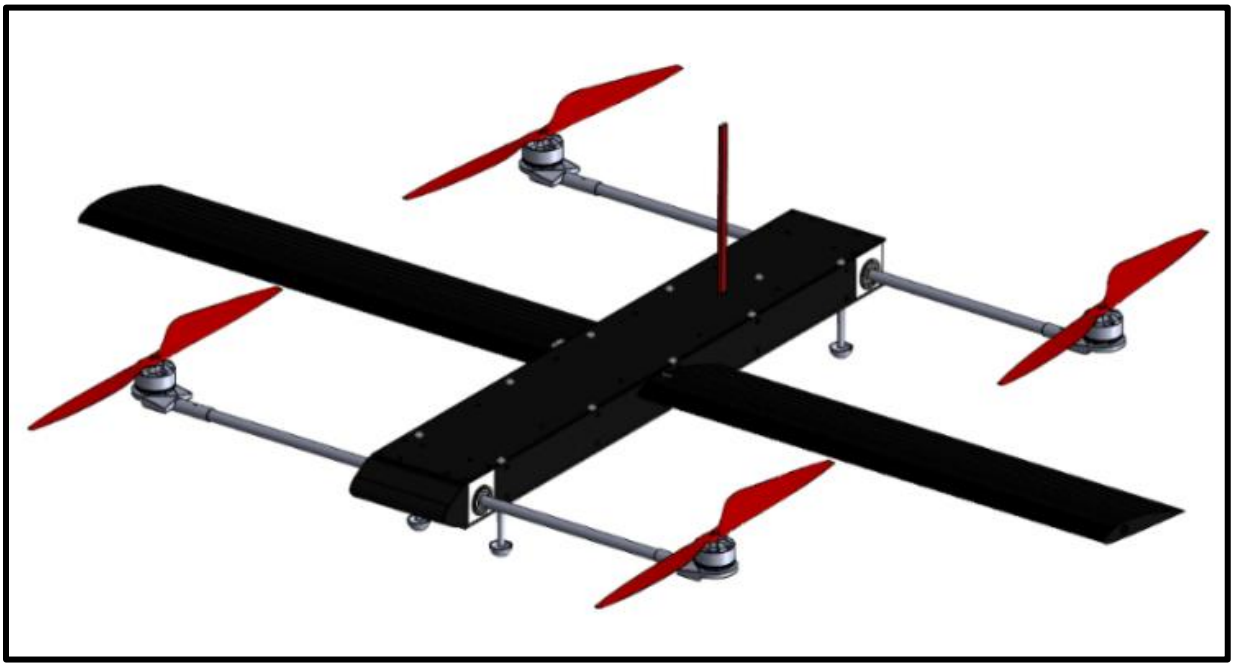

Figure 1: Isometric view of aircraft in vertical flight

Management Summary

To design and build an eVTOL aircraft, a diverse team is required. Buckeye Vertical aimed to build a unique team of individuals, which includes a variety of disciplines and class standings. The versatility in background the team has allows the team to design, construct, and test an eVTOL aircraft to meet the specific challenges set forth by the Design-Build-Vertical Flight Competition. The specific demands of the competition led Buckeye Vertical to form three sub-teams: Structures, Software, and Avionics. Each sub-team has focused on individual elements of the aircraft design as well as component integration. Team organization has been implemented to synergize the output of each sub-team, leading to a cohesive final design. Each sub team has one lead that oversees their group. When a task requires multiple sub teams, the groups work together to come up with the best solution. The team organization is shown in Figure 2.

When looking at the Gantt chart in Figure 3, the second half of the project started on December 20th with continued work on the aircraft and the start of the final technical report. The code for the aircraft was beginning to be developed at the same time. By March, most of the parts arrived and the build of the aircraft began. Towards the end of March and start of April the aircraft was to be finished along with the final technical report. Flight testing and work on the presentation followed the completion of the aircraft. The tasks were able to be put into four main categories: conceptual design, detailed design, fabrication, and testing. The conceptual design started on December 20th and went until the draft outline for the final technical report. That is when the detailed design started and went until the 3-D blocks were printed. Fabrication started with the blocks being made and the parts being cut to size. The final category, testing, started once the drone was fully assembled and was able to be tested.

Adithya Ramaswami
Role: President & Team Lead
Major: Aerospace Engineering - 4th Year
VFS ID: 23867

Dr. Jim Gregory	Dr. Matthew McCrink
Role: Advisor	Role: Advisor
Department Chair of Mechanical and Aerospace Engineering at The Ohio State University	Research Scientist, Aerospace Research Center
VFS ID: 2377	VFS ID: 118081

Structures Team

Michael Valcarcel	Patrick Brandt	Tanner Sabau	Rachel Younkin	Gio Ranieri
Role: Vice President & Structures Lead	Role: Aerospace Lead	Role: Team Member	Role: Professional Development Chair & Team Member	Role: Treasurer & Team Member
Major: Mechanical Engineering - 1st Year	Major: Aerospace Engineering - 3rd Year	Major: Aerospace Engineering - 1st Year	Major: Aviation Management - 3rd Year	Major: Aerospace Engineering - 1st Year
VFS ID: 23113	VFS ID: 23912	VFS ID: 23923	VFS ID: 23913	VFS ID: 23919

Software Team

Pete Park	Chris Johnson	Rachit Aggarwal
Role: Software Team Lead	Role: Air Mobility Symposium Liaison & Team Member	Role: Consultant & Team Member
Major: Biomedical Engineering - 1st Year	Major: Aviation Engineering - 2nd Year	Major: PhD Student & Graduate Research Associate
VFS ID: 23915	VFS ID: 23924	VFS ID: 23926

Avionics Team

Alex Houston	Gaven Zou	Jake Ferris	Mitchell Kaminski
Role: Avionics Team Lead	Role: Structural Analysis Lead	Role: Team Member	Role: Team Member
Major: Aerospace Engineering - 3rd Year	Major: Aerospace Engineering - 3rd Year	Major: Aerospace Engineering - 2nd Year	Major: Mechanical Engineering - 1st Year
VFS ID: 23746	VFS ID: 23920	VFS ID: 23925	VFS ID: 23922

Figure 2: Team organizational chart

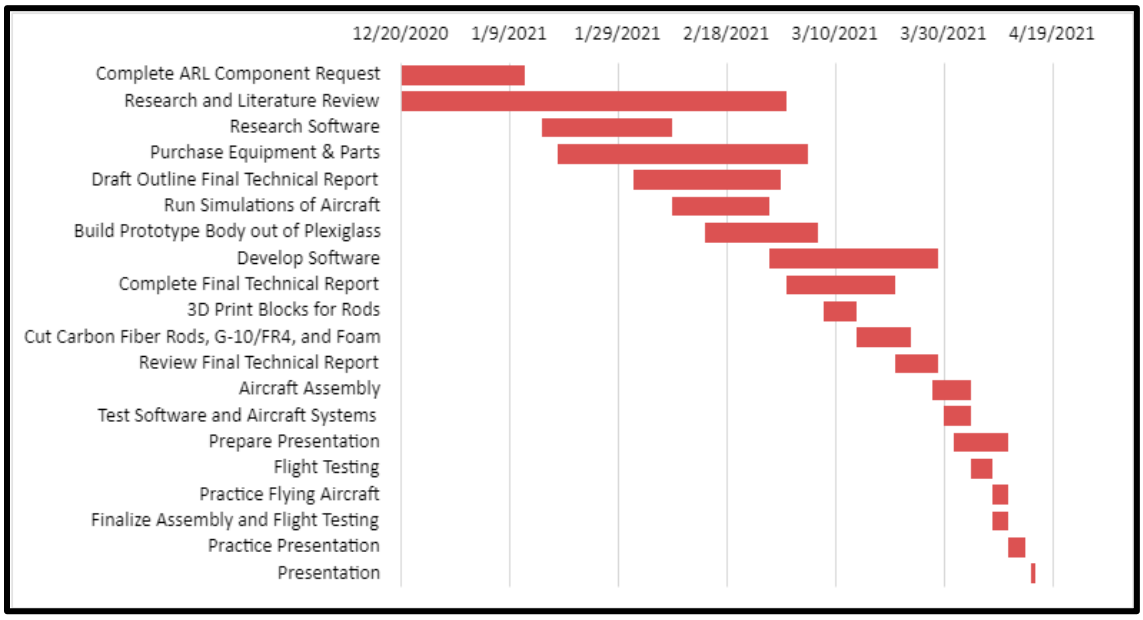

Figure 3: Gantt chart

Design Trade Studies

The scoring rubric was analyzed to understand the specific competition challenges that had the largest points awarded for completing them. A house of quality of vehicle configurations was developed to narrow down the most favorable aircraft design in terms of the competition scoring areas. The design requirements dealing with the competition tasks with the largest payout were given the highest relative weight. With these tasks, there were certain aircraft components that directly impacted the points scored. The payload fraction is the payload weight divided by the aircraft's total weight, the payload included. The best payload fraction can be attained by minimizing aircraft weight while still being able to complete the basic mission, and then if able, adding extra payload. Going for a larger payload would likely require more weight on the aircraft, but additionally, going for a larger heavier aircraft makes the weights of small components less impactful. A 12 lb drone capable of carrying 6 lb would score the same as a 4 lb drone carrying 2 lb (0.5 payload fraction). For the endurance challenge, the aircraft will be scored based on the number of laps it can complete in 10 min. To complete the maximum number of laps in the allotted time for the endurance course, two elements of the aircraft were identified – battery consumption and speed. Table 1 below depicts a house of quality of design considerations and was used as a foundation to narrow down the final vehicle configuration.

Table 1: House of quality of vehicle configurations

			Vehicle Configurations		
		Direction of Improvement	▲	□	□
Relative Weight	Competition Payouts	Design Requirements	Quad-Copter	Hexa-Copter	Tilt Rotor Fixed Wing
15%	8	Payload Capacity	○	●	●
7%	4	Weight of Aircraft	○	▽	●
16%	9	Battery Consumption	○	▽	●
13%	7	Agility	●	●	○
18%	10	Max Forward Flight Speed	▽	○	●
9%	5	Take off and Landing	○	●	●
11%	6	Stability	○	○	●
5%	3	Pilot Control	●	●	○
4%	2	Software Complexity	○	○	●
2%	1	Mechanical Complexity	▽	▽	●
		Importance Rating Sum (Importance x Relationship	369,0909091	500	790,9090909
		Final Weight Percentage	22%	30%	48%

With these requirements targeted for the aircraft, there were multiple candidate designs discussed, including a traditional quadcopter, hexacopter, and a tilt rotor quadcopter with a fixed-wing. The quadcopter alone does not provide the most optimal results when considering efficiency due to the vertical thrust component from the motors having to lift the full weight of the aircraft [1]. Although the hexacopter has the potential to provide more thrust compared to the quadcopter, the hexacopter's 6 rotors would also require more power, decreasing the efficiency of the aircraft and the time available to complete the endurance challenge [2]. The tilt rotor quadcopter with a fixed-wing allows for the lift produced by the wing to reduce the vertical component of thrust required from the rotors, increasing efficiency by decreasing power consumption and yielding more flight time [3]. Lastly, the tilt rotor mechanism allows the front two rotors to rotate in the direction of forward flight to quickly increase horizontal speed.

After taking all these factors into account, a quadcopter design with a tilt rotor mechanism on the front was chosen, using an H-frame design. The aircraft would be a larger scale at near 10 lb unloaded. This weight allows for adequate battery sizing for the endurance challenge and if provided enough power the aircraft can score a maximum payload fraction of 1/2. A wing attached to the aircraft with a span near the maximum allowed dimension of 6 ft will provide a large amount of lift to the aircraft.

For the tilt rotor and fixed wing configuration to improve scoring in the endurance competition, the required power must be reduced enough to allow for the battery to last through all 10 min of flight. Of course, maximizing the battery capacity and thus size will ensure battery does not run out; however, the aircraft configuration can reduce the battery size needed to complete the 10 min of flight. The primary parameter affecting power consumption is the motor thrust, so reducing the cruising thrust is prioritized. Since minimizing weight may have negative implications in payload fraction scoring, the use of a wing is a more optimized means of decreasing the required vertical thrust. With the addition of a fixed wing, the vertical thrust is reduced as the wing generates lift to counter the aircraft's weight. The tilting rotor maximizes the efficiency gained from the wing by allowing the aircraft to fly with its fuselage parallel to the oncoming air. This orientation reduces drag, which reduces the required horizontal rotor thrust. Additionally, the horizontal flight attitude will allow the wing angle of attack to be optimized, maximizing efficiency in vertical thrust reduction.

Given the frequent acceleration and deceleration required to complete the courses and the ability to safely operate the aircraft, it was decided that the aircraft will have a target maximum horizontal speed of 40 feet per second (ft/s). This will yield a competitive speed to complete the courses while maintaining a safe speed the pilot could control. Additionally, a target hover time of 11 min was set to ensure the aircraft maximized the full 10 min of flight during the endurance course.

Technical Innovations

With the difficult vehicle configuration selected, the team relied on brainstorming innovative sub-assemblies that could solve the complexities of the selected design. After identifying the need for a tilt rotor and fixed wing, the team transitioned to developing solution concepts through the engineering design process. This required the team to iterate through many cycles of designing, prototyping, and testing to develop technical innovations for the tilt rotor mechanism and wing design.

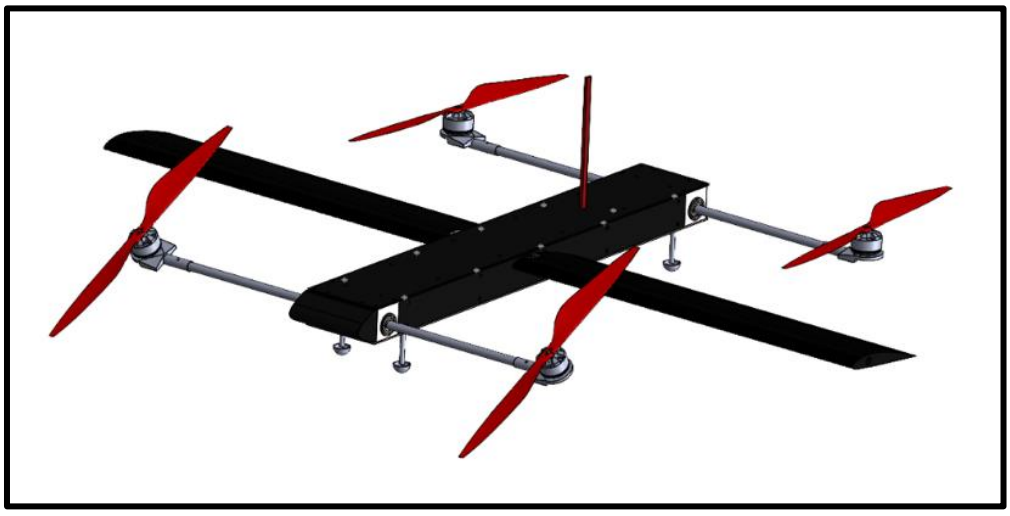

Figure 4: Isometric view of aircraft in forward flight

Tilt Rotor

The tilting rotor aircraft configuration comes with many challenges; however, the concept is expected to meet the competition objectives with high performance. A primary challenge of the design is flight vehicle control during

transitioning flight between vertical and horizontal flight modes. As the front rotors tilt forward, the thrust of the front rotors must increase such that the vehicle remains level with the ground. Additionally, the subsystem required for tilting the front rotor adds weight, mechanical, and avionics complexity to the aircraft. Finally, the fixed wing will reduce maneuverability and vertical flight efficiency. These obstacles are some of the trade-offs accepted in favor of the aircraft's boosted efficiency and endurance performance.

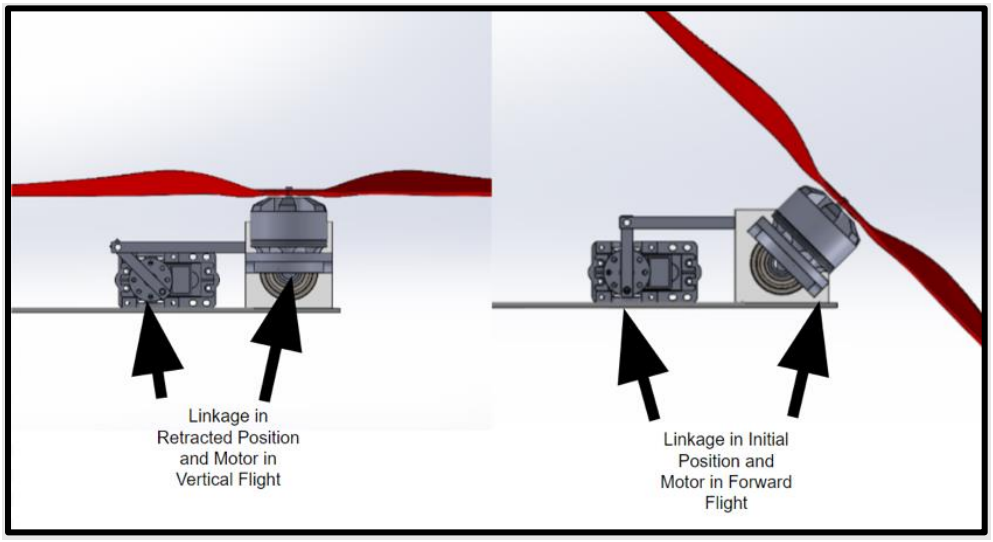

Figure 5: Tilt rotor with linkage assembly

Some methods of accounting for the challenges of the aircraft configuration are outlined on the following pages. The arm that supports the front rotors will be rotated about their longitudinal axis to orient the motors in different directions in-flight. This will allow the front two motors to be angled during forward flight and vertical for takeoff and landing operations. The angled motors will significantly increase vehicle range by allowing the aircraft to fly forward with a reduction in required total thrust, due to the fixed wing. The arm rotation mechanism will consist of a servo attached to a linkage bar that will engage during the transition to forward flight.

As the rotors tilt forward, an equal vertical thrust must be generated between the front rotors and the rear rotors. When the vertical thrust is not balanced between the front and rear rotor arms, the aircraft pitch will change. The goal of the tilting rotor aircraft is to fly with level pitch. This relationship is displayed below in Equation (1), which relates the thrust of the rear rotors (T_r) with the thrust of the front rotors (T_f) and the angle of tilt between the front rotors and the vertical position (β).

$$T_r = T_f \cos(\beta) \tag{1}$$

Thus, as the front rotor angle increases, the front rotors must produce more thrust for fixed rear thrust. Alternatively, as the wing generates lift for the aircraft, the front and rear rotors will generate less vertical thrust.

Wing Design Approach

To reduce the required thrust from the rotors during cruising flight, the team incorporated a fixed wing to provide part of the vertical force needed to balance the aircraft's weight in forward flight. This lifting force would contribute to the aircraft's power efficiency and maximum range by reducing the required thrust of the rotors. Equation (2) shows the relationship between the required vertical force of the rotors (F_v) to the aircraft weight (W) and wing lift (L) for steady flight. Maximizing the wing's lift will minimize the vertical force of the rotors and thus minimize batter consumption. Thus, a high lift coefficient cross section is prioritized.

$$F_v = W - L \tag{2}$$

For the wing's shape, many airfoils were considered from the NACA 4 series and the NACA 6 series. The distance between the front and back rotors limited the wing's chord length to 6 in. Since the wing's lift is directly

proportional to its planform area, the maximum chord length was chosen. After simulating flow over airfoils of thicknesses between 10% and 18% chord with XFLR5, the airfoil geometry was chosen based on maximum lift coefficient and lift to drag ratio. The NACA 4313 airfoil was chosen for its maximum lift coefficient of 1.5 at 12 degrees angle of attack and its high lift to drag ratio. The software predicted a maximum lift to drag ratio of around 50; however, this is an overestimate since the software was used to predict two-dimensional flow. In flight, the wing is expected to have an induced drag, reducing the lift to drag ratio. The cross section of the airfoil is shown below in Figure 6. The two-dimensional XFLR5 predictions are shown in Figure 7 below.

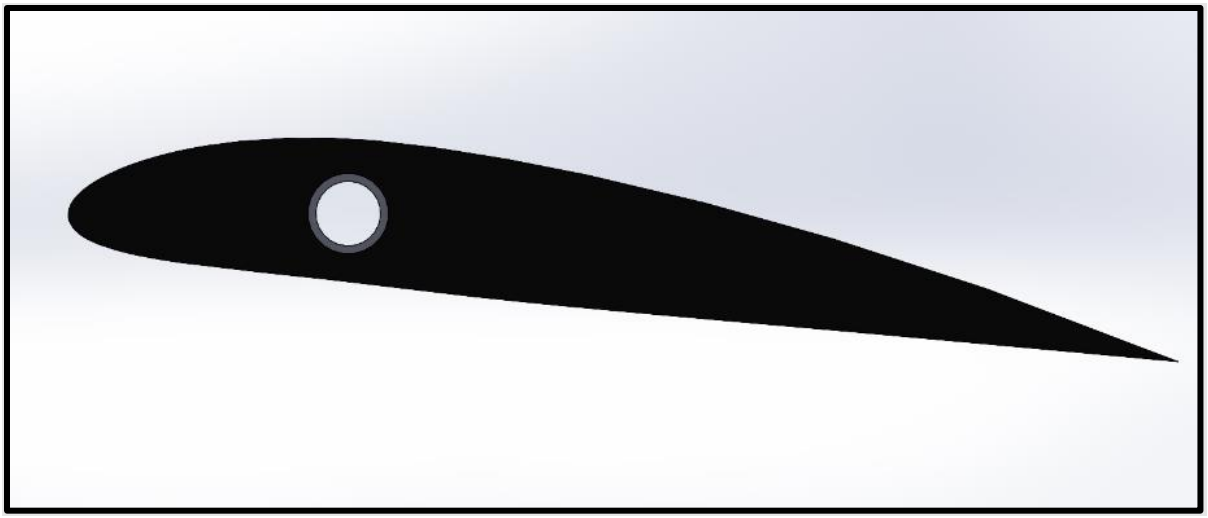

Figure 6: Cross-section of airfoil

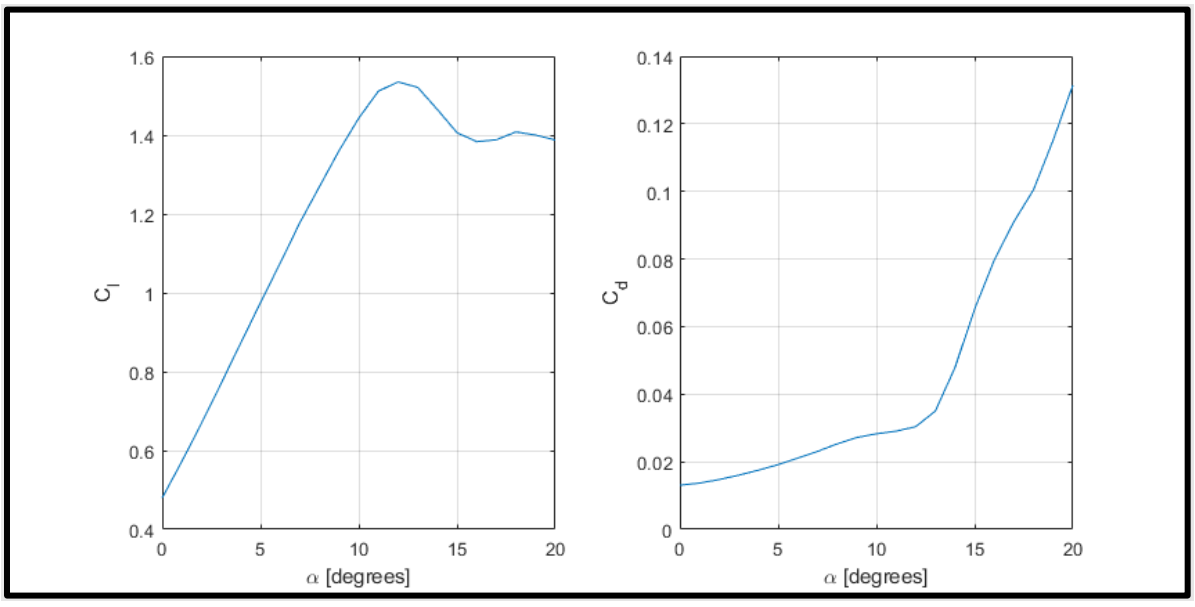

Figure 7: XFLR5 prediction of lift and drag variation with angle of attack for NACA 4313

Based on the XFLR5 prediction, the wing is installed at an angle of 8 degrees, where the lift to drag ratio for the wing is predicted to reach its maximum value of 50. At this angle, the expected lift coefficient is 1.27, and the drag coefficient is 0.025. Additionally, the wing is predicted to stall at 12 degrees angle of attack, so the 8-degree installation will provide a safe error margin for practical piloted flight. Since the analysis of Figure 7 incorporates a two-dimensional prediction, the lift-to-drag ratio is an overprediction. With a three-dimensional prediction, the expected lift-to-drag ratio for the wing is 16.

Mission Model

For all competition flights, time and energy should not be wasted on climbing any higher than required. For both missions, height of cruise is chosen to be 15 ft above ground level (AGL). This is higher than the minimum height of 5-6 ft set for the competition so that slight errors can be corrected. This height should be attained quickly to avoid unnecessary time spent in hover, which is inefficient and wastes time that could be spent moving horizontally.

The below graph shows how the time to reach an altitude of 15 ft varies with different vertical thrust values on the aircraft. The times were attained by finding the acceleration of the aircraft via Newton's second law for many forces (thrust minus weight) with 12 lb mass (lb_m) and then using the accelerations found to calculate when the aircraft would reach 15 ft in height.

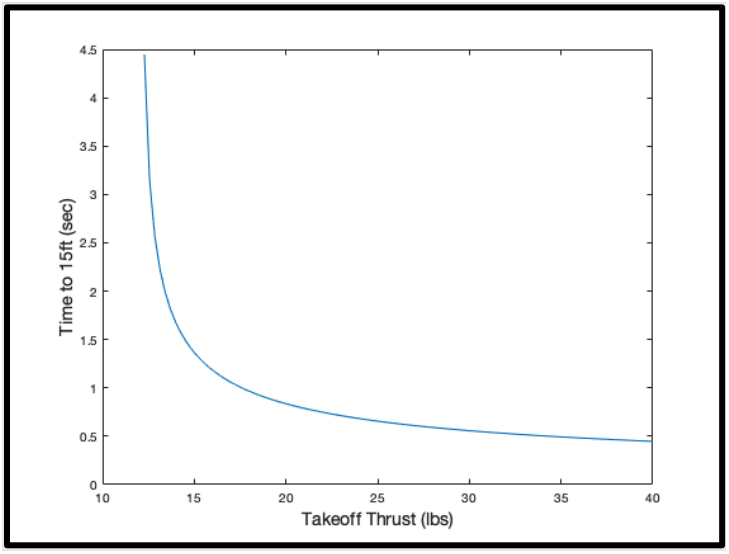

Figure 8: Time to reach cruise altitude

Increasing the thrust decreases the aircraft's time to climb to 15 ft; however, Figure 7 shows that as takeoff thrust continues to increase, the rate of change of time-to-climb with respect to thrust is decreasing. In other words, increasing thrust yields diminishing returns for time-to-climb. Common multirotor design practice is to have at least 1.5 to 2.0 times the weight of the aircraft in thrust. The maximum thrust value of 24 lb meets this rule of thumb and provides an expedient climb to cruise height.

Transition to horizontal flight from the vertical climb involves rotating the forward motors into the forward direction. During this rotation, throttle on the two forward motors will increase relative to the rear to maintain a balance of vertical thrust, as a portion of the total forward motor thrust becomes horizontal.

After this transition completes, as horizontal speed increases the lift provided by the wing will also increase. With more lift, less thrust and battery power need to be used. A maximum cruise speed of 40 ft/s was chosen to allow the vehicle to still be easily controllable while still covering significant distance quickly.

A very conservative drag coefficient of 1.5 was chosen to ensure that even if inefficiencies occur where conditions are less than ideal, the aircraft will still comfortably be able to reach its target speed. Considering the cruise speed of 40 ft/s, assuming sea level air density, and a wing area of 2 ft, the calculation below yielded the required horizontal thrust for cruising flight to be 5.7 lb at this speed. Equation (3) shows the required horizontal force of the front rotors (F_h) as it depends on air density (ρ), wing area (S), and drag coefficient (C_D).

$$Drag = \frac{1}{2}\rho v^2 S C_D = 5.7\ lb \tag{3}$$

Additionally, it is required that the net vertical force on the aircraft be balanced during horizontal flight between the motors and the wing. The tilt rotor configuration requires the front rotors to produce all the horizontal thrust in addition to one half of the vertical thrust, while the remaining one half of the vertical thrust is provided by the rear rotors. The remaining vertical force will be provided by the wing.

While the back rotors will produce 4 lb of vertical thrust, the front rotors will tilt forward. The front rotors will produce a combined force with a horizontal component of at least 5.7 lb and a vertical component of 4 lb, balancing the rear rotors. This configuration requires a total front-rotor force of 6.2 lb. Thus, each front rotor is required to develop a 3.1 lb force at an angle of 54.9 degrees from vertical. Additionally, the wing will provide the additional 4 lb of lift to total the 12 lb of vertical force need.

$$\tan^{-1}(5.7lb/4lb) = 54.9°$$

Using these thrust values, the equations of motion were solved to analyze expected performance in forward fight stretches. The equations of motion are shown below (Equations 4 and 5); a solution was evaluated based on the cruising horizontal thrust value of 5.7 lb. The equations relate the mass (m) and acceleration ($\dot{v}$) of the aircraft to horizontal rotor force and aircraft drag. Equation (4) is used for acceleration and cruise while Equation (5) is used for deacceleration.

$$m\dot{v} = (F_h - \frac{1}{2}\rho v^2 S C_D) \tag{4}$$

$$m\dot{v} = (-F_h - \frac{1}{2}\rho v^2 S C_D) \tag{5}$$

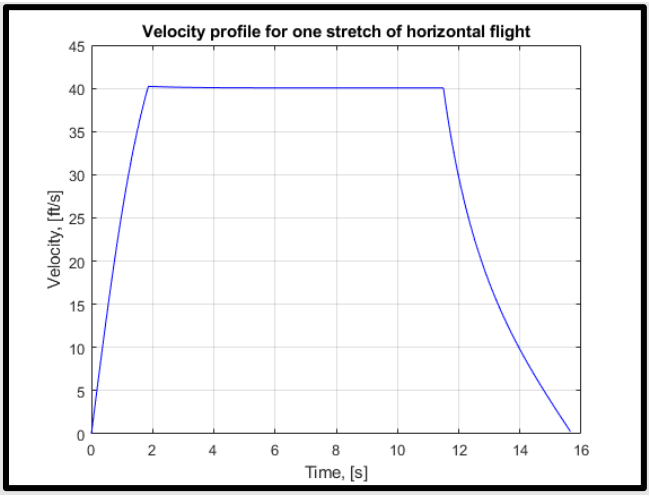

Figure 9: Velocity profile numerical solution for 500 ft stretch of straight flight

The distance traveled over time is represented by the area under the curve in Figure 9. As an example, the profile above represents flight over 500 ft in roughly 16 s. The solution assumes a transition towards deaccelerating flight at 11.5 seconds (s); however, this will ultimately be an input of the pilot. The velocity profile type can be used to model expected performance in the maneuverability competition, as the course's maximum stretch of flight is 500 ft. A time of fewer than 16 s to complete the stretch of 500 ft was deemed competitive within safe operating speeds.

To transition into vertical landing, the reverse of the earlier transition occurs as the forward motors reduce their excess thrust as they rotate to vertical. After this is finished, a flare maneuver is executed to quickly reduce horizontal speed while maintain altitude. At a 60 degree angle with motors producing 24 lb of thrust the vehicle will stop from 40 ft/s within 3.4 s with a horizontal force of 20.8 lb.

$$\cos^{-1}(12lb\ /24lb) = 60°$$

Finally, the aircraft will descend from the 15 ft cruise height in a controlled manner at approximately 2 ft/s, slowing at a few feet from the ground. The landing operation should take about 10 s.

This model assumes that winds will be low, that thrust availability is constant throughout the flight and that maneuvers will be performed precisely. In reality, there will be a chance for wind to affect flight, available thrust will decrease as the batteries drain, and the pilot will not be perfectly precise in their flying.

Design Definition

Aircraft Dimensions and Materials

The aircraft has a wingspan of 55 inches and has a length of 31 inches. The total height of the aircraft is 6 inches, and the fuselage is 5 inches wide. The booms for the motors and the wing spar are made of carbon fiber, the fuselage is made of G-10/FR4 plate material, the wing is foam core formed with fiberglass, and the structural blocks are 3-D printed PLA. The materials were chosen for their light weights, while retaining necessary strength and rigidity for flight.

Stability

For static stability, it is beneficial that the aircraft center of gravity is located at an equal distance from each rotor, so this is planned for the design. The center of gravity can be easily adjusted after manufacturing by changing the installation of batteries or payload.

According to XFLR5, the center of pressure of the three-dimensional wing will be at 40 percent chord. On the aircraft, this means that the center of pressure will be close to 2 inches behind the wing's leading edge, assuming that the wing's contribution to the center of pressure location dominates. Another condition for longitudinal static stability is that the aircraft's aerodynamic center is aft of the center of gravity. Alternatively, it can be required that the aircraft center of pressure is coincident with the center of gravity for trimmed flight [4]. With these considerations in mind, the wing will be installed where space allows between the rotors, with the wing's leading edge approximately 2 inches front of the center of gravity. After applying these rules to the aircraft design, it is reasonable to expect longitudinal static stability from the aircraft. Software in the control loop can also add to the aircraft's static stability.

For dynamic stability, there are many more parameters affecting aircraft performance, including the flight mode. One component that plays a role in dynamic stability is the rotor radius. The rotor radius is proportional to system stability; increasing the rotor radius has positive effects on dynamic stability for the aircraft. This is true for ranges of rotor radius such that the rotor radius is smaller than the length between a rotor center and the aircraft's center of gravity. Outside of this range, it is possible for turbulence effects between propellers to compound [5]. With this knowledge, the rotor radius is prioritized for vehicle design.

Weight and Balance

The total weight of the aircraft without payload is 11.85 lb. This is 1.85 lb greater than the model weight, but the motors selected have enough extra thrust to counter the small amount of additional weight added. The aircraft still has a thrust to weight ratio of 2.35, meeting the industry minimum standard of 1.5 to 2.0. The payload which will be on the top plate will be placed such that the center of gravity will be located vertically in line with the flight controller, which is in the geometric center of the fuselage. Having the center of gravity located forward of the approximate aerodynamic center contributes to positive stability of the aircraft.

Structural Analysis

The most significant forces are the thrust forces from the motors, which will be carried through the carbon fiber boom, into the structural blocks within the fuselage, which are sandwiched between the fuselage plates. The maximum expected force for each motor is 8.2 lb. The spar internal to the wing will help maintain flexural rigidity of the wing. A maximum vertical force of 5.5 lb and horizontal force of 2 lb will be transferred from the wing and spar into the fuselage plates.

The following structural design calculations presents the maximum load scenarios for the G-10/FR4 frame, for bolted-joint analysis, and for the carbon fiber support strut strength. The max g-force was determined by considering the lightest aircraft scenario, which would be the aircraft itself without any payload. A max g-force of 2.75G is considered longitudinally, laterally, and vertically for the calculations and is calculated below in Equation (6), where $G\ Force_{max}$ is the max G-Force, T_{max} is the max thrust of the aircraft, and $W_{aircraft}$ is the weight of the aircraft.

$$G\ Force_{max} = \frac{T_{max}}{W_{aircraft}} = 2.75\ G \tag{6}$$

When deciding which sheet material to use for the fuselage frame, the team analyzed both the G-10/FR4 and STD Carbon Fiber materials, as shown by the table below [6].

Table 2: Material specification - comparing G-10/FR4 & STD carbon fiber sheets

Specification	**G-10/FR4 Material**	**STD Carbon Fiber Material**
Tensile Strength	40,000 psi (ASTM D638)	87,000 psi
Shear Strength	19,000 psi (ASTM D732)	43,500 psi (half of tensile)
Compressive Strength	60,000 psi (ASTM D695)	82,670 psi
Flexural Strength	55,000 psi (ASTM D790)	44,200 psi
Material Density	0.065 lb/in^3	0.060 lb/in^3

The team chose to use G-10/FR4 instead of the originally planned carbon fiber for the frame. G-10/FR4 is seven times cheaper and is more than sufficient for the maximum expected loads on the airframe as shown by the structural analysis below. The densities for G-10/FR4 and carbon fiber are also relatively similar, with the G-10/FR4 having a slightly higher density of 0.005 lb/in^3 in difference from the carbon fiber. As a result, the overall increase in mass of 0.26 lb_m (from 52 in^3 total sheet volume) of the aircraft is minute when factoring in cost savings of seven times the money on the G-10/FR4 sheet material as opposed to carbon fiber sheets.

The L-Brackets connecting the G-10/FR4 fuselage sheets were also analyzed for their tearout stresses from the 1/8" inner diameter (ID) screws. The following calculation in Equation (7) shows the bearing area stress (tearout) for a total quantity of 12 L-Brackets, where $\sigma_{b,\ L-Bracket}$ is the bearing area stress for the L-bracket, $W_{payload}$ is the weight of the payload, $n_{b,\ L-bracket}$ is the quantity of bearing area L-brackets, and $A_{b,\ L-Bracket}$ is the bearing area consisted of the thickness of the L-bracket and the screw ID.

$$\sigma_{b,\ L-Bracket} = \frac{W_{aircraft} + W_{payload} + (G\ Force)}{n_{b,\ L-bracket} * A_{b,\ L-bracket}} = 399.2\ psi \tag{7}$$

The bearing area (tearout) stress for the G-10/FR4 sheets from the 1/8" inner diameter screws were then calculated in a similar fashion. Equation (8) shows the tearout stress, where $\sigma_{b,\ sheet}$ is the bearing area stress for the sheet, $n_{b,\ sheet}$ is the number of sheets bearing areas, and $A_{b,\ sheet}$ is the bearing area consisted of the thickness of the sheet and the screw ID.

$$\sigma_{b,\ sheet} = \frac{W_{aircraft} + W_{payload} + (G\ Force)}{n_{b,\ sheet} * A_{b,\ sheet}} = 798.4\ psi \tag{8}$$

The screws for attaching the L-Brackets to the fuselage frame were then analyzed to determine their max tensile and shear stresses for the aircraft. The following shows a table for the aluminum 1/8"(T) L-Bracket material specifications [7].

Table 3: Material specification - bolted-joint analysis on aluminum screws

Specification	**Aluminum Material**
Yield Tensile Strength (YTS)	40.000 psi
Yield Shear Strength (Von-Mises Yield Criterion)	23,080 psi (0.577 * YTS)

Equation (9) shows the max tensile and shear stress calculations for a quantity of 12 screws, where σ_{max} is the max tensile stress, τ_{max} is the max shear stress, n_{screw} is the number of screws, and $A_{screw,\ cross-section}$ is the cross-sectional area of the screw.

$$\sigma_{max} = \tau_{max} = \frac{W_{aircraft} + W_{payload} + (G\ Force)}{n_{screw} * A_{screw,\ cross-section}} = 508.3\ psi \tag{9}$$

As for the support strut rods that connect the motors and propellers to the fuselage, the team decided to go with carbon fiber since it was a strong and lightweight material that would span across the entire lateral width of the aircraft. The following shows a table for the 0.472" OD, 0.39" ID, carbon fiber rod material specifications [8].

Table 4: Material specification - carbon fiber rod (boom)

Specification	**Carbon Fiber Rod Material**
Tensile Strength	120,000 psi
Compressive Strength	75,000 psi
Flexural Strength	89,000 psi

With 89,000 psi as the flexural strength, the carbon fiber support strut rods (booms) were analyzed to compare the maximum allowable force (on one side of a single rod) to the actual calculated force for the aircraft design. Equation (10) takes in the flexural strength of 89,000 psi and calculates $F_{allowable,\ center\ of\ rod}$, the allowable force at the center of the rod, where $\sigma_{F.S.}$ is the flexural strength, and $A_{rod,\ cross-section}$ is the cross-sectional area of the rod.

$$F_{allowable,\ center\ of\ rod} = \sigma_{F.S.} * A_{rod,\ cross-section} = 4940.8\ lb_f \tag{10}$$

Equation (11) then finds allowable pressures, where $P_{allowable,\ center\ of\ rod}$ is the max allowable pressure at the center of the rod, $P_{allowable,\ end\ of\ single\ rod}$ is the max allowable pressure at the end of a single rod (motor and propeller location), and $d_{moment\ arm}$ is the moment arm distance.

$$P_{allowable,\ center\ of\ rod} = P_{allowable,\ end\ of\ single\ rod} = \frac{F_{allowable,\ center\ of\ rod}}{d_{moment\ arm}} = 449.17\ psi \tag{11}$$

The max allowable force at the end of a single rods (motor and propeller location) were then calculated in Equation (12), where $F_{allowable,\ end\ of\ single\ rod}$ is the max allowable force at the end of a single rod.

$$F_{allowable,\ end\ of\ single\ rod} = P_{allowable,\ end\ of\ single\ rod} * A_{rod,\ cross-section} = 274.3\ lb_f \tag{12}$$

The combined forces at the end of a single rod were then found in Equation (13), which was necessary to compare to its allowable value. $F_{end\ of\ single\ rod}$ represents the calculated combined forces at the end of a single rod, W_{motor} is the weight of the motor and $W_{propeller}$ is the weight of the propeller.

$$F_{end\ of\ single\ rod} = W_{motor} + W_{propeller} + (G\ Force) = 1.9015\ lb_f \tag{13}$$

From the force calculations at the end of a single rod, as shown above, the aircraft's calculated force at the end of a single rod, 1.9015 lb_f is far below the carbon fiber's max allowable flexural force at the end of a single rod, 274.3 lb_f. The lightweight carbon fiber rod can withstand much more weight than current configuration.

The bending moment, $M_{bending}$, of the carbon fiber rods was also calculated in Equation (14) to help show how much bending may occur to the aircraft's booms from the forces applied along the carbon fiber rods, where $n_{thrust\ units\ per\ rod}$ is the number of thrust units on a single rod.

$$M_{bending} = n_{thrust\ units\ per\ rod} * F_{end\ of\ single\ rod} * d_{moment\ arm} = 41.83\ lb_f - in \quad (14)$$

The 3-D printed PLA blocks that hold the booms (rods) also needed to be analyzed for its tearout strength properties. Out of the two options, the team decided to use PLA instead of ABS since its material strengths were higher. Being made from PLA, the block material strength is less than the rod's flexural strength; as a result, the PLA block material is the limiting factor for how much thrust the aircraft can provide before rod tears out of the block. The yield tensile strength of the PLA material is 3782.87 psi (26.082 MPA) according to "3DPrint" testing results [9]. For analyzing 3-D printed PLA, the team utilized the yield tensile strength and reduced it a factor of two for its calculations to account for the 3-D printing's crosshatch/weave patterns; this ultimately would result in the need to consider the "shear" strength of the printed blocks (assumed half of tensile). Equation (15) shows a conservative calculation (from edge of rod instead of center to edge of block) for $\tau_{\ tearout,\ block}$, the tearout shear stress of the block, with n_{block} being the number of blocks per boom (rod), $n_{shear\_surface,\ block}$ being the number of shear surfaces to consider per block, and $A_{shear\_surface,\ block}$ being a single shear surface area (1.5" thickness, 0.4" distance from the edge of the THRU-hole to edge of the block) for tearout analysis.

$$\tau_{\ tearout,\ block} = \frac{W_{aircraft} + W_{payload} + (G\ Force)}{n_{block} * n_{shear\_surface,\ block} * A_{shear\_surface,\ block}} = 31.19\ psi \quad (15)$$

As shown by the tearout stress calculations, the expected max shear in the aircraft is less than "half of the yield tensile strength" which is 1891.43 psi for the PLA material; the PLA blocks will be strong enough to withstand the thrust and G-Forces associated during flight.

Propulsion System

Propeller, Motor, and Electronic Speed Controller (ESC)

The T-motor P22x8 carbon fiber propeller has a disk area of 2.64 ft^2, meaning the aircraft's disk loading is 1.14 pounds per square foot (lb/ft^2) by using Equation (16). This calculation includes the estimated loaded aircraft weight of 12 lb. The lower disk loading value provides increased efficiency in hover flight. According to manufacturer specifications [10] the configuration at 70% throttle will produce 3.7 kg of thrust per propeller, resulting in a total of 32.6 lb of thrust. This will produce the required thrust to obtain at least the target thrust to weight ratio of 2.

$$Disk\ Loading = W/(4 * Single\ Rotor\ Disk\ Area) \quad (16)$$

The T-motor MN6007 320 rotations per min per volt (KV) has a large radius stator size which provides a range from zero to 1.1 newton-meters (N·m) torque to rotate and accelerate the chosen propeller. A brushless motor was chosen instead of a brushed motor due to its greater efficiency, power, and durability. This motor's efficiency ranges from 6.42 to 11.59 grams per Watt (g/W), with power up to 780 Watt (W). According to manufacturer's specifications, each motor draws 20.64 amps at 70% throttle with a 22 inches propeller.

The T-Motor F45A 3-6S BLHeli32 ESC can carry a continuous current draw of 45 amps and a burst current draw of 55 amps. This is sufficient for the selected motors' current draw (programmed maximum 70% throttle) estimation given by the manufacturer's specifications [10] The ESC can handle maximum 55 amps of continuous current draw, allowing for 62% current headroom to ensure no failure of the ESC occurs during maximum power operation.

Batteries

In order to provide the power to the system, the Turnigy 4500 milliamp-hours (mAh) 6S 25C LiPo battery was selected to power the propulsion system. The chosen battery capacity (*Cb)* of 99.9 Watt-hours (Wh) is less than the competition limitation of 100 Wh. Two of these batteries are to be wired in parallel in accordance with competition rules (including fuses and a shunt plug) for a total of 199.8 Wh, providing a flight time of 12.6 min. This time was calculated by Equation (17) when flying with 5.3 lb of thrust referencing the motor datasheet for current draw [10]. The battery weighs 1.44 lb and provides 22.2 Volts (V). The available current of the battery is 112.5 amps per battery shown via Equation (18). When combined in parallel, the batteries provide a greater available current draw for the motors at maximum power. Current demand from the motors is represented by (*Ad*).

$$Flight\ Time\ (mins) = (Cb)/(Ad) * (60\ min) \quad (17)$$

$$Battery\ Available\ Current = (C\_rating) * (Cb) \quad (18)$$

As required by competition rules, a separate battery was selected for the flight controller and certain avionic components. The flight controller battery was chosen to be a Turnigy 450 mAh 3s 60 C-rating (C) LiPo battery. Weighing 0.112 lb, the battery provided an energy density of 97.94 Watt-hour per kilogram (Wh/kg). Based on PixHawk's 2.5 W power consumption, the battery will give the flight controller 2 hours of operation, which is well above the required maximum flight time of 10 min. This will provide full avionics capability for an extended period when the aircraft is idled, such as for testing or for mission preparation.

Servo

The Hexfly 25KG High Torque Waterproof Servo's purpose is to rotate the forward motor arm. This servo provides a torque of 2.1 N·m at 5 V of power which will be used with a gearing system to rotate the forward motor arms in flight.

Avionics

Flight Controller

A major scoring objective was to utilize a flight controller to have a stable and assisted flight for both manual and autonomous operations. The PixHawk 4 flight controller provides a platform to use for autonomous flight mission planning. The flight controller's wide selection of external aiding sensors allowed for various data from each accessory to be received; the Global Positioning System (GPS), compass, Light Detection and Ranging (LIDAR), telemetry, and airspeed sensor allow for an accurate autonomous mission.

For external data, the LIDAR, airspeed, GPS, and compass data are each measured with a Garmin LIDAR, a Holybro Airspeed Sensor, and a Neo M8N GPS. The airspeed data will be utilized to support the tilt rotor mechanism. The data from the LIDAR will be utilized to support autonomous landing and take-off and assist with isolation from the ground effect produced by the propellers when flying close to the ground.

Telemetry and Radio Control (RC)

Using the DSMX protocol in the 2.4 gigahertz (GHz) frequency, the aircraft's radio control system consists of the Spektrum RC transmitter paired with a Spektrum DSMX receiver. The use of a different frequency from the telemetry link will help prevent radio-frequency interference. A DSMX SRXL2 serial receiver with telemetry will be used for up to 20 channels of control and mixing.

Telemetry data is transmitted using the Holybro Micro Transceiver Telemetry Radio Set on the 915 megahertz (MHz) frequency band using 100 milliwatts (mW) of power via Mavlink for PC ground control and display. Frequency-hopping spread spectrum aids with noisy radio frequency environments.

First Person View system (FPV)

For manual maneuverability, it is difficult to control an aircraft's line of sight due to the aircraft's tilt rotor mechanism. An FPV system's camera aids onboard controls using a camera so the pilot can see altitude, movement, and essential telemetry data of the aircraft. A visual observer (VO) is required to be present with the remote pilot in command for situational awareness. The FatShark HDO2 FPV goggles were chosen to be used by the team in conjunction with diversity patch and circular antennas to ensure strong video signal reception.

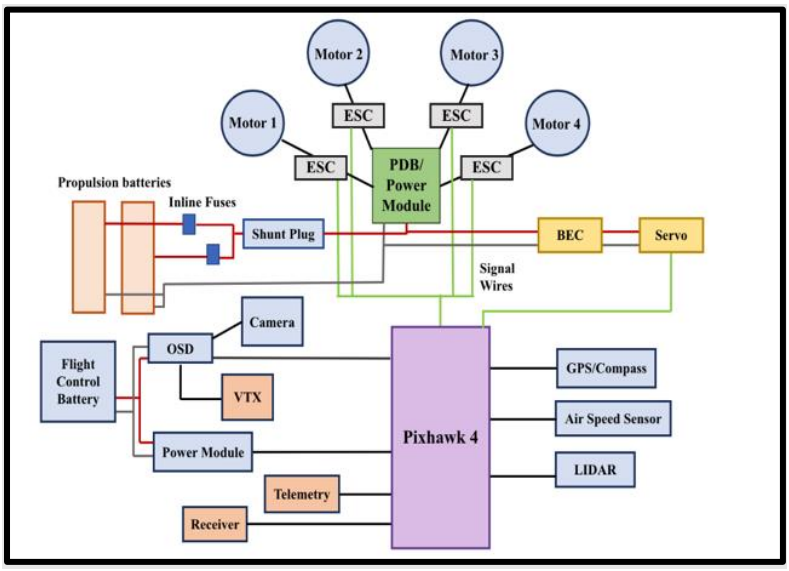

Figure 10: PDB/Power module diagram

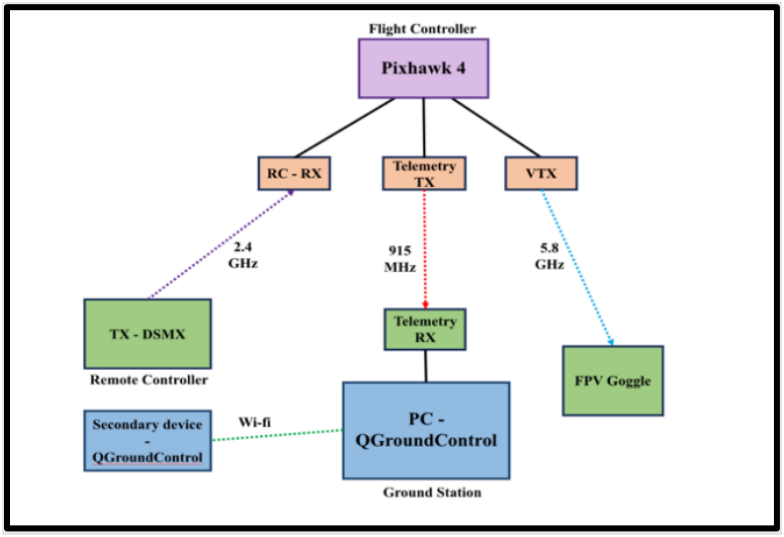

Figure 11: Pixhawk 4 flight controller diagram

Software

A Pixhawk 4 flight controller (PX4) is needed for the aircraft stability and control, with or without autonomous control programming. For the autonomous flight challenge, the software needed to be the primary control method for executing the autonomous mission plan. For manual flight, the PX4 interprets remote control signals and sends new throttle signal to the motors. There is currently no existing firmware that fully supports the team's aircraft tilt rotor design, and the team had to implement further code to accommodate the aircraft's control and autonomy aspects. Without the customized PX4 software implemented, the aircraft would act like a standard quadcopter and not take full advantage of the fixed wing design to provide maximum lift at an optimal speed.

The PX4 can be configured to a custom airframe to suit the aircraft. The approach to the team's software design was to combine aspects of both multi-rotor and fixed-wing airframe software to help achieve tilt rotor transition (varying tilt rotor angle) as well as autonomy. Within the current PX4 software, the team chose the "VTOL-Tilt rotors" configuration, which combines multi-rotor and fixed-wing aspects, to support tilt rotor transition. The PX4 software also helps the pilot transition from vertical to horizontal flight and vice versa; the software then inputs rates (radio input) to the "VTOL attitude controller" and transposes data to the mixer. Custom PX4 mixer code is then used for stability purposes to allocate the amount of thrust and motor/propeller tilt from the servo. The mixer code also helps

dampen and adjust gains so that the system is stable rather than becoming unstable. The tilt rotor mixer incorporates the control allocation matrices to compensate for the loss of vertical thrust from the varying-angled tilt rotors, resulting in the need for an increase in motor power.

To test the aircraft virtually, the modified code and configuration is simulated in Gazebo which can be used with Software-in-the-Loop (SITL) to simulate tilt rotor configurations and the autonomous mission plan. QGroundControl is used to configure the drone, as well as to upload the mission plan. The Gazebo simulation then sends simulated flight data to the running SITL. After inputting data such as the attitude setpoint, flight mode, test density, weight, and geometry of the aircraft into the Gazebo, the team assessed the simulation to further analyze the aircrafts' flight performance for the mission plan, adjusting inputs and tunings as needed in an iterative design process.

Mission Performance

Lift and Drag Performance

When the aircraft is in forward flight, the total lift and drag forces can be estimated by Equations (19) and (20), where L represents the lift force and D represents the drag force. W is the aircraft weight.

$$L = W = L_{rotors} + L_{wing} = T_{v,rotors} + \frac{1}{2}\rho v^2 S_{wing} C_{L,wing} \tag{19}$$

$$D = T_{h,rotors} = D_{fuselage} + D_{wing} = \frac{1}{2}\rho v^2 (S_{fuselage} C_{D,fuselage} + S_{wing} C_{D,wing}) \tag{20}$$

Because the wing is installed on the aircraft at 8 degrees, the expected wing lift coefficient will be 1.3, and the wing drag coefficient will be 0.025 from Figure 7. These figures were generated for the wing design using the software package XFLR5. Given the fuselage geometry, the drag coefficient is calculated to be 0.3 [11]. The horizontal thrust required for flight at 40 ft/s (equivalent to drag at that speed) is estimated as 2.0 lb. Similarly, the expected wing lift will be 5.5 lb, so the rotors will need to produce a total of 6.5 lb of vertical lift. This estimation shows that the designed wing provides a significant reduction in the required vertical thrust of the rotors, as a quadcopter would be required to produce 12 lb of vertical thrust in addition to a horizontal thrust with a wingless configuration.

Maneuverability Performance

There are a total of 4 takeoff and landing operations within the maneuverability course, and 1354 ft of horizontal distance must be covered. Using times estimated in the model, the estimated total time to complete the course can be calculated. With the previously calculated takeoff and landing times of 0.7 s and 10 s respectively, the time to complete comes to 76.7 s.

$$4(0.7\ s + 10\ s) + \frac{1354\ ft}{\left(\frac{40 ft}{s}\right)} = 76.7\ s$$

Endurance Performance

Assuming a generous turning radius of 50 ft, the aircraft must cover a distance of 1,114 ft per lap of the endurance course. The lap time can be calculated to be 38.6 s per lap. With this lap time the number of full laps that can be completed within the allotted 10 min is 15 laps.

$$(0.7\ s + 10\ s) + \frac{1114\ ft}{\left(\frac{40 ft}{s}\right)} = 38.6\ s$$

$$\frac{600\ s}{(38.6\ \frac{s}{lap})} = 15.5\ laps$$

Drawing Package

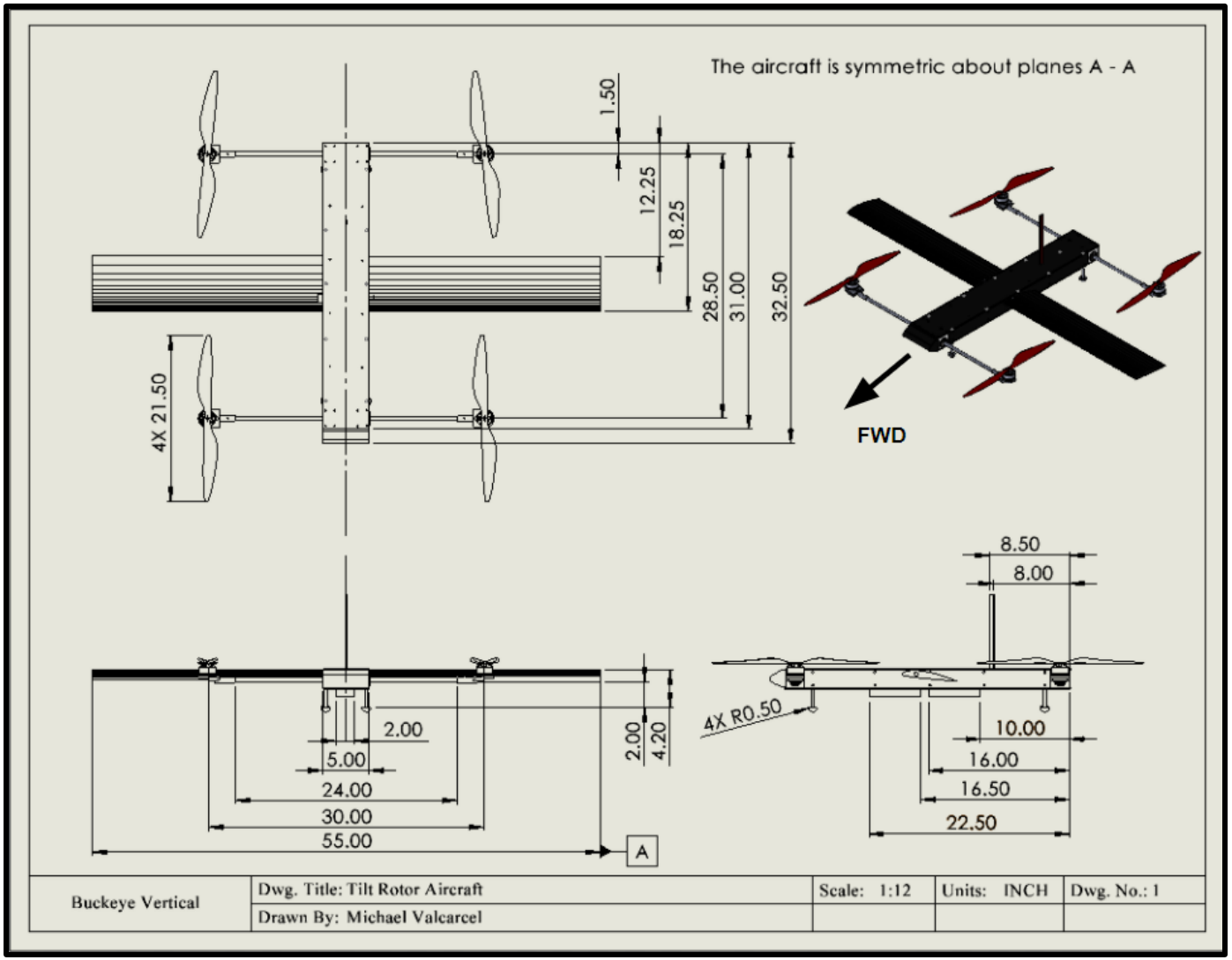

Figure 12: Engineering drawing of aircraft

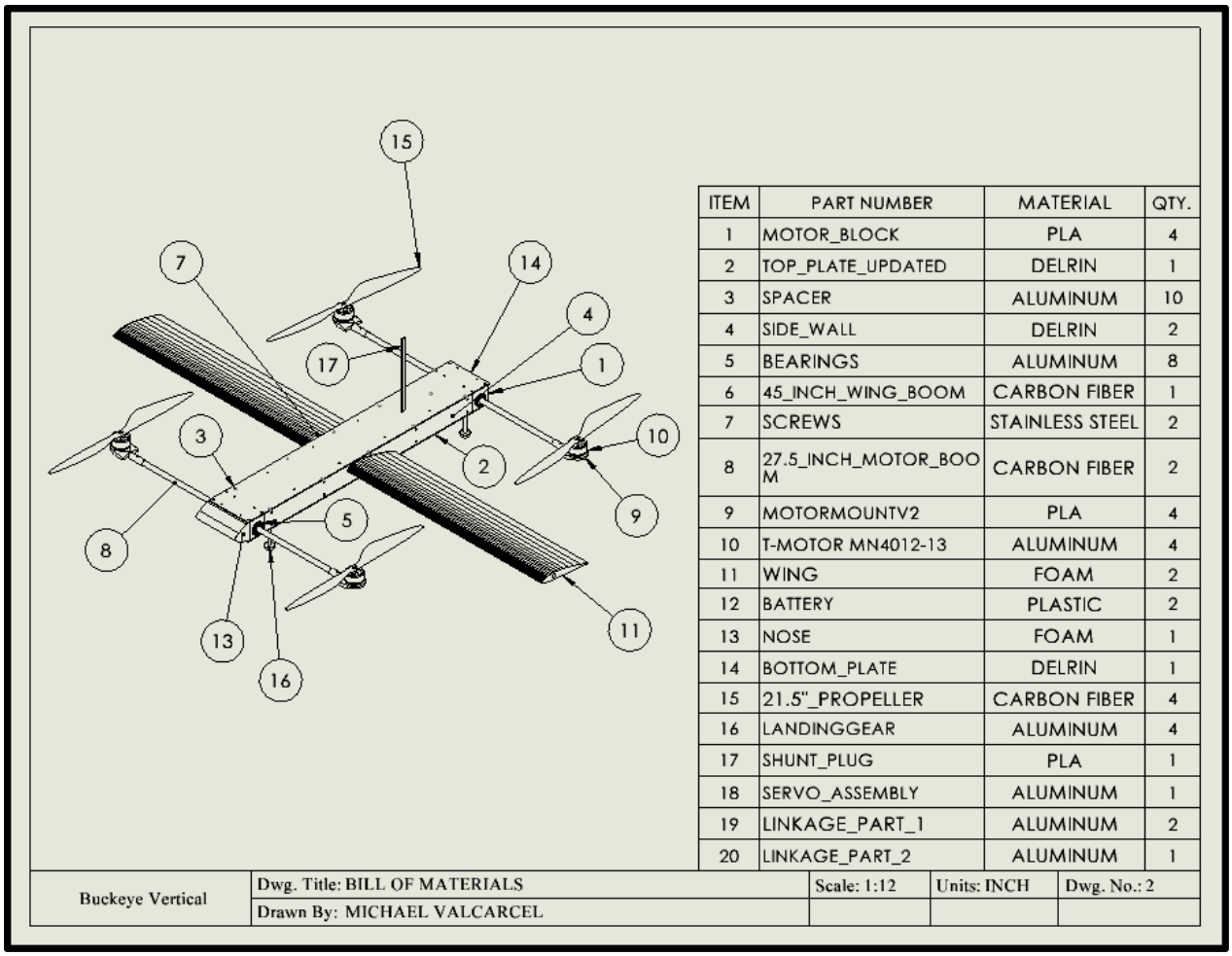

ITEM	PART NUMBER	MATERIAL	QTY.
1	MOTOR_BLOCK	PLA	4
2	TOP_PLATE_UPDATED	DELRIN	1
3	SPACER	ALUMINUM	10
4	SIDE_WALL	DELRIN	2
5	BEARINGS	ALUMINUM	8
6	45_INCH_WING_BOOM	CARBON FIBER	1
7	SCREWS	STAINLESS STEEL	2
8	27.5_INCH_MOTOR_BOOM	CARBON FIBER	2
9	MOTORMOUNTV2	PLA	4
10	T-MOTOR MN4012-13	ALUMINUM	4
11	WING	FOAM	2
12	BATTERY	PLASTIC	2
13	NOSE	FOAM	1
14	BOTTOM_PLATE	DELRIN	1
15	21.5"_PROPELLER	CARBON FIBER	4
16	LANDINGGEAR	ALUMINUM	4
17	SHUNT_PLUG	PLA	1
18	SERVO_ASSEMBLY	ALUMINUM	1
19	LINKAGE_PART_1	ALUMINUM	2
20	LINKAGE_PART_2	ALUMINUM	1

Buckeye Vertical	Dwg. Title: BILL OF MATERIALS	Scale: 1:12	Units: INCH	Dwg. No.: 2
	Drawn By: MICHAEL VALCARCEL			

Figure 13: Engineering drawing of structural arrangements with bill of materials

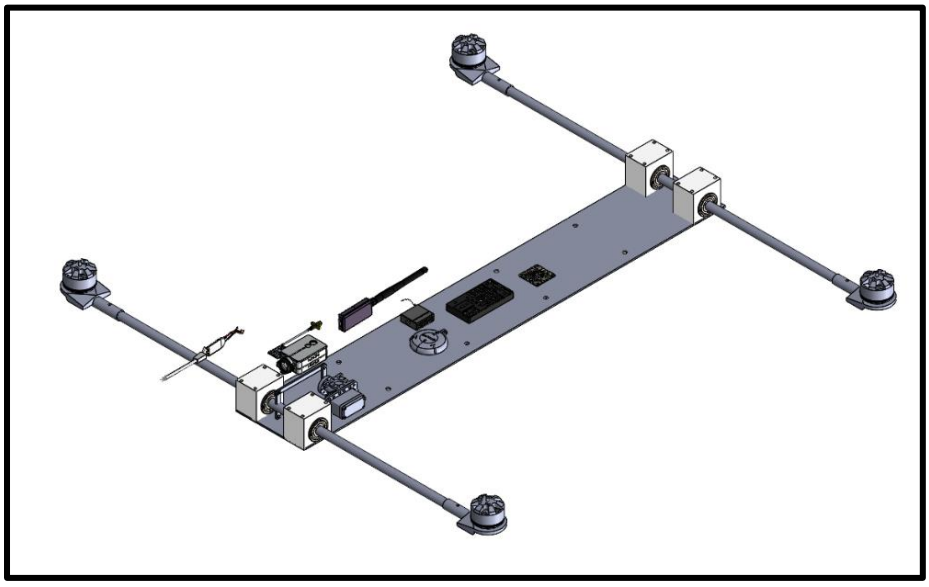

Figure 14: Isometric view of systems layout

Fabrication Methods

Several leading manufacturing techniques were considered in the planning of the aircraft fabrication process. These manufacturing techniques include laser cutting, 3-D printing, workshop tooling, plexiglass prototyping, hot wire foam cutting, and soldering. Laser cutting was considered for its precision while having power to cut through the materials utilized.

Fuselage

The G-10/FR4 plates were cut using a CNC machine. These cut locations were given to the CNC machine by a drawing file, so the cuts very precisely matched the CAD design. This reduced the potential for human error and gave clean cuts for the fabrication of the fuselage.

A 3-D printer printed parts and brackets that were not purchasable. Some printed parts include brackets to hold the batteries under the aircraft, blocks made to hold the four ball bearings for the rods, and motor mounts. 3-D printing is a relatively cheap and easy way to produce parts quickly and reduced time needed to implement a design change.

Common shop tools such as circular saw, drill press, and band saw will be used for assembly of the aircraft. The prototype fuselage plate will be made from plexiglass rather than G-10/FR4 because it is cheap and easy to mark and cut. This layout allows for planning and marking of where cuts will be and where components would go without damaging the final fuselage. Once everything is marked out on the plexiglass, the final fuselage components are cut out and put together.

Wing

The wing is constructed from an airfoil shaped foam cutout, and then sandwiched between two layers of composite hardened with resin. A foam core wing wrapped in composite provides comparable strength to molded composite wing for much less time, cost, and complexity. For this build process, the first step is to cut the wing shape out of foam. Since foam had to be cut, research into hot wire cutting was made to ensure smooth clean cuts were made on the foam so the carbon fiber can easily be applied.

Electronics

Soldering would be used to facilitate connection between the electronic components. A soldering iron and metal solder are used when soldering. The soldering iron melts the solder to create a conductive connection between two electrical conductors, in the form of wires, connectors, or copper pads.

Materials

The materials chosen for the aircraft were weighted against other possible candidates and were picked primarily by comparing strength with density, as well as the cost. The rods of the aircraft for the motors and the wing spar will be made of carbon fiber. Carbon fiber was picked over aluminum due to it being much lighter [12] while still having a good amount of strength and stiffness [13].

The blocks that that hold the carbon fiber motor booms are 3-D printed from PLA. Though Delrin Blocks would be stronger and were initially a part of the design, they are much heavier than the 3-D printed blocks and harder to fabricate.

It was determined that the body of the aircraft is made from G-10/FR4 over carbon fiber due to them being very similar in properties but G-10/FR4 is much cheaper than carbon fiber. G-10/FR4 is made by stacking multiple layers of glass cloth and then soaking in epoxy resin. It is then cured under heat and pressure to make highly durable sheets. The use and benefits of G-10/FR4 are described in more detail on reference website [14].

The wing composite material is a carbon fiber weave. Carbon fiber is made by weaving together small fibers that are mostly comprised of carbon atoms. This results in a very lightweight material that is very strong and stiff, which are crucial characteristics when creating a durable and strong wing.

Test Plan

A system operational test will be performed without the propellers attached to verify that all systems perform as expected. This includes checking the accuracy of the LIDAR sensor, verifying the motors spin in the right direction, ensuring the telemetry readings are correct, and FPV radio frequencies are set properly. A range test for the primary control signal, telemetry signal, and FPV signal will be performed. For the range test, the aircraft should have stable telemetry, video, and control signal in all orientations at least 1000 ft away from the ground station. This is assessed by carrying the aircraft to this distance (still with propellers removed for safety). Signal strength can be assessed via the received signal strength indicator (RSSI) by recording flight computer data and by viewing video through FPV goggles.

After the system operational test is successful, a flight test will be performed. The first will be a simple hover to verify stability. The aircraft should be able to remain in one place, without the center drifting out of a 6 ft diameter circle for one min in winds less than 18 mph (a moderate breeze, according to the Beaufort wind estimation scale). This will be followed by a flight without tilting the forward motors. In this configuration, the aircraft will fly at least 600 ft away from the ground station to again verify stability of control, video, and telemetry signals. After success in the preceding test, the forward motors will be tilted and an attempt to reach 40 ft/s will be made.

For final testing, an approximation of the endurance and maneuverability courses will be used to attempt the missions. Additionally, an autonomous flight will be made to verify successful operation of the autonomous mission programming. All flight tests will be performed in conformance with all 14CFR Part 107 regulations and all other relevant laws. The pilot will have a spotter at all times. Data from the tests will be recorded on the flight computer for analysis.

Flight Test Results

The team was only able to begin working in-person towards the end of February due to COVID-19 restrictions on campus. Despite limited in-person meetings this competition season, the team will continue to build the aircraft after the FTR is submitted and iterate on the design. Below are steps that the team would have taken towards documenting and utilizing flight test results.

Three sets of flight tests will be used for validation of the aircraft and its subsystems. The first set will serve as an extension of the individual static tests. Hover tests and forward flight tests will be used to demonstrate the proper performance of the propulsion and electrical systems. Stability and control of the aircraft will be observed during turn tests, and takeoff/landing tests when the transition from vertical to forward flight occurs. These tests will be used to tweak different components of the aircraft.

The next set of test flights will focus on payload directed flights. Payload weight will be increased while the aircraft's flight ability was monitored to identify the maximum payload capacity amidst maintaining the aircrafts flight characteristics. This will provide the maximum payload fraction for the competition.

References

[1] Shastry, Abhishek Kumar, et al. "Generalized Flight Dynamic Model of Quadrotor Using Hybrid Blade Element Momentum Theory." *Journal of Aircraft*, vol. 55, no. 5, Sept. 2018, pp. 2162–68., doi:10.2514/1.C034899.

[2] Zhu, He, et al. "Design and Assessment of Octocopter Drones with Improved Aerodynamic Efficiency and Performance." *Aerospace Science and Technology*, vol. 106, Nov. 2020, p. 106206., doi:10.1016/j.ast.2020.106206.

[3] Traub, Lance W. "Optimal Battery Weight Fraction for Maximum Aircraft Range and Endurance." *Journal of Aircraft*, vol. 53, no. 4, July 2016, pp. 1177–79., doi:10.2514/1.C033416.

[4] Anderson, John D. *Introduction to Flight*. Eighth edition, McGraw-Hill Education, 2016.

[5] Yunping Liu, et al. "Structural Stability Analysis and Optimization of the Quadrotor Unmanned Aerial Vehicles via the Concept of Lyapunov Exponents." *International Journal of Advanced Manufacturing Technology*, vol. 94, no. 9–12, Feb. 2018, pp. 3217–3227. *EBSCOhost*, doi:10.1007/s00170-016-9311-z.

[6] Turla, P., Kumar, S. S., Reddy, H. P., & Shekar, C. K. (2014). Processing and Flexural Strength of Carbon Fiber and Glass Fiber Reinforced Epoxy-Matrix Hybrid Composite. *International Journal of Engineering Research & Technology (IJERT), 3*(4).

[7] Cavallo, C. (n.d.). All about 6061 aluminum (properties, strength and uses). Retrieved March 28, 2021, from https://www.thomasnet.com/articles/metals-metal-products/6061-aluminum/#:~:text=6061%20aluminum%20alloy%20has%20a,310%20MPa%20(45000%20psi).

[8] McMaster-Carr. (n.d.). Carbon Fiber Tube, 0.465" OD, 0.39" ID, 72" Long. Retrieved March 23, 2021, from https://www.mcmaster.com/2153T129/

[9] Saunders, S. (2019, January 18). Researchers investigate tensile properties of 3d Printed PLA Specimens: Is 80% INFILL best? - 3DPrint.com: The voice of 3d printing / additive manufacturing. Retrieved March 28, 2021, from https://3dprint.com/233916/tensile-properties-of-3d-printed-pla/#:~:text=%E2%80%9CIt%20has%20resulted%20in%20the,yield%20strength%20of%2026.082%20MPa.&text=%E2%80%9CThe%20tensile%20properties%20of%20PLA,strain%20graphs%20upon%20tensile%20tests.

[10] "*TMOTOR"*, store-en.tmotor.com/h5/.

[11] National Aeronautics and Space Administration. (2015, May 5). Shape Effects on Drag. Retrieved March 23, 2021, from https://www.grc.nasa.gov/www/k-12/airplane/shaped.html

[12] Psyclops - Density of materials. (n.d.). Retrieved March 23, 2021, from http://www.psyclops.com/tools/technotes/materials/density.html

[13] Performance Composites. (2009). Mechanical Properties of Carbon Fibre Composite Materials, Fibre / Epoxy resin (120°C Cure). Retrieved March 23, 2021, from http://www.performance-composites.com/carbonfibre/mechanicalproperties_2.asp

[14] G-10/FR-4 (glass cloth / EPOXY RESIN). (2012, June 14). Retrieved March 23, 2021, from http://sterlingplasticsinc.com/materials/g-10fr-4-glass-cloth-epoxy-resin/